Pertanika J. Sci. & Technol. 31 (4): 1717 - 1729 (2023)

PERTANIKA JOURNALS

SCIENCE & TECHNOLOGY

Journal homepage: http://www.pertanika.upm.edu.my/

Effect of Transition Metals Addition on the Nickel Oxide Catalyst Toward Reduction Behaviour in Carbon Monoxide Atmosphere

Norliza Dzakaria[1], Azizul Hakim Lahuri[2]*, Fairous Salleh[3], Tengku Shafazila Tengku Saharuddin[4], Alinda Samsuri[5] and Mohd Ambar Yarmo[3]

[1]Advanced Material for Environmental Remediation (AMER) Research Group, Faculty of Applied Science, University Teknologi MARA, Cawangan Negeri Sembilan, 72000 UiTM, Kuala Pilah, Negeri Sembilan, Malaysia

[2]Department of Science and Technology, Universiti Putra Malaysia Bintulu Campus, 97008 UPM, Bintulu, Sarawak, Malaysia

[3]Catalysis Research Group, Department of Chemical Sciences, Faculty of Science and Technology, Universiti Kebangsaan Malaysia, 43600 UKM, Bangi, Selangor, Malaysia

[4]Faculty of Science and Technology, Universiti Sains Islam Malaysia, 71800 USIM, Nilai, Negeri Sembilan, Malaysia

[5]Department of Chemistry, Centre for Defence Foundation Studies, Universiti Pertahanan Nasional Malaysia, 57000 UPNM, Kuala Lumpur, Malaysia

ABSTRACT

The chemical reduction progression behaviour of transition metals (Mo, Zr, W, Ce, and Co) doped on NiO was studied using temperature programmed reduction (TPR) analysis. A wet impregnation method was applied to synthesise the doped NiO series catalysts. The reduction progress of the catalysts was attained by using a reductant gas at the concentration of 40% v/v CO/N_2. X-ray diffraction (XRD) was employed to determine the composition of the reduced phases. Undoped NiO was reduced at 384°C to obtain a cubic phase of NiO. It was observed that Ce/NiO exhibited the lowest reduction temperature of 370°C among all catalysts. This phenomenon might be due to a higher surface area of Ce/NiO compared to undoped NiO, which facilitated a faster reduction reaction. The rest of the doped NiO series catalysts (Co/NiO, Mo/NiO, W/NiO and Zr/NiO) demonstrated a higher reduction temperature compared to undoped NiO. New peaks in the XRD pattern were observed only for the reduced catalysts of Mo/NiO and W/NiO, which were associated with monoclinic MoO_2 and $WO_{2.72}$ phases, respectively. The formation of new compounds or more stable nickel

ARTICLE INFO

Article history:
Received: 16 June 2022
Accepted: 16 August 2022
Published: 24 May 2023

DOI: https://doi.org/10.47836/pjst.31.4.07

E-mail addresses:
norliza864@uitm.edu.my (Norliza Dzakaria)
azizulhakim@upm.edu.my (Azizul Hakim Lahuri)
fairoussalleh@gmail.com (Fairous Salleh)
tengkushafazila@usim.edu.my (Tengku Shafazila Tengku Saharuddin)
alinda@upnm.edu.my (Alinda Samsuri)
ambar_y@gmail.com (Mohd Ambar Yarmo)
* Corresponding author

ISSN: 0128-7680
e-ISSN: 2231-8526

alloys led to a slower reduction reaction than undoped NiO. Therefore, Ce/NiO was the most efficient catalyst in promoting the formation of Ni under the CO atmosphere.

Keywords: Carbon monoxide, metal oxide, nickel oxide, nickel, reduction

INTRODUCTION

The transition-metal oxides (TMOs) fascinate the materials chemists ascribed to the interesting class of inorganic metals (Ahmad et al., 2022). Their magnetic (Farber et al., 2014), electrical (Rebello & Adeyeye, 2016), optical (Pandey et al., 2020), catalytic (Zheng et al., 2013) and mechanical properties (Vazinishavan et al., 2018) are the significant features in various applications. TMOs are compounds of oxygen atoms bound to transition metals, commonly utilised in several electronic applications due to their superior semiconducting properties (Parkinson et al., 2010; Kaiser, 2004). TMOs have important physical properties in which the spinal oxides show comparably good, interesting magnetic and electrical properties (Cho et al., 2017). These features make TMOs very attractive for several novel applications.

Recently, nanostructured materials have been noticed by researchers owing to their unique and fascinating properties. Specifically, metal oxide nanomaterials, such as NiO, have attracted interest and are applied in various technologies and industries. Nickel oxide is a prominent example of TMO. It is also used as a catalyst in CO_2 capture (Hakim, Tahari et al., 2015; Hakim, Isahak et al., 2015; Lahuri et al., 2022) and as antiferromagnetic layers in lightweight structural components in the aerospace, in active optical filters, in cathode materials for alkaline batteries and materials for gas or temperature sensors, such as CO sensor, H sensor, and formaldehyde sensors (Khan et al., 2019). Besides, the performance of the TMOs, namely CeO_2 and Co_3O_4, was also proven in other applications, such as CO_2 capture (Lahuri et al., 2020). Meanwhile, MoOx, ZrOx and WoOx catalytic activities in hydrogen production were also explored (Sun et al., 2020; Fakeeha et al., 2020; Oudejans et al., 2022; Wondimu et al., 2022).

The performance of Ni-based catalysts is significant as metal oxide support (Charisiou, Papageridis et al., 2019; Charisiou, Tzounis et al., 2019; Papageridis et al., 2020). For instance, alkali and alkaline earth metals (Tsiotsias et al., 2020), transition metals (Lv et al., 2020) and rare-earth metals (Siakavelas et al., 2021) have proven their suitability as promoters through modification of physicochemical properties of metal oxide support (Anastasios et al., 2021). The co-deposition of CeO_2 and NiO can improve the corrosion resistance compared to pure Ni (Hasannejad et al., 2012). A comparison from previous work showed that NiO as bimetal catalysts of nickel oxide exhibited a high reduction temperature in the CO atmosphere as the percentage of zirconia and cobalt increased (Dzakaria, Samsuri et al., 2020; Dzakaria, Tahari et al., 2020).

Therefore, this work attempted to study the influence of the reduction behaviour of NiO doped with transition metals such as Ce, Co, Mo, W and Zr. The catalysts were reduced using carbon monoxide to obtain the reduction pattern with their reduction temperature.

MATERIALS AND METHODS

Catalyst Preparation

The NiO (97.0%) and $(NH_4)_2Ce(NO_3)_6$ (99.0%) were purchased from Acros Organics and Merck. $Co(NO_3)_2{\cdot}6H_2O$ (99.0%), $(NH_4)_6Mo_7O_{24}{\cdot}4H_2O$ (99.98%), $(NH_4)_{10}H_2(W_2O_7)_6{\cdot}xH_2O$ (99.99%) and $ZrOCl_2{\cdot}8H_2O$ (98.0%) were purchased from Merck, Sigma-Aldrich, Aldrich Chemistry and Acros Organics respectively. The ethanol was obtained from Systerm®. The wet impregnation method prepared the Ce/NiO, Co/NiO, Mo/NiO, W/NiO, and Zr/NiO catalysts. Three per cent wt./wt. Ce, Co, Mo, W and Zr of the total metal cation were dissolved in 5 mL distilled water and 5 mL ethanol. The NiO powder was added corresponding to the metal cation additives in the above proportion. The mixture was stirred aggressively for 2 hours at room temperature. The mixtures were dried at 120°C overnight and subsequently calcined at 400°C for 4 hours. The catalysts were denoted as Mo/NiO, Zr/NiO, W/NiO, Ce/NiO and Co/NiO.

Characterisation

The TPR analysis was performed by using a Micromeritic Autochem 2920 Chemisorption Analyzer. The 50 mg of catalysts were heated up with non-isothermal reduction until 700°C at 10 °C/min and followed by isothermal reduction at 700°C for 60 minutes with 40% CO in N_2 flow at 20 mL/min (STP) was introduced as reducing gas. The CO consumption was detected by a thermal conductivity detector (TCD) in the instrument. The structures' lattices and phases were identified using the XRD Bruker AXS D8 Advance type. The X-ray radiation source was Cu K_α (40 kV, 40 mA), and the 2θ diffraction was recorded at the angle of 10-80º with the wavelength of $\lambda = 0.154$ nm. The XRD patterns were matched with standard diffraction (JCPDS) to determine the crystalline phase composition.

The N_2 adsorption-desorption isotherms and textural properties were obtained using a static volumetric technique instrument (Gas sorption analyser, Micromeritics ASAP 2020). The Brunauer-Emmett-Teller (BET) surface area was calculated from the isotherms. Approximately 500 mg of catalysts were outgassed at 300°C for 4 hours under vacuum to remove moisture content and humidity gases before measurement. The measurement was conducted in a circulating bath of liquid N_2 of nitrogen (77 K).

RESULTS AND DISCUSSION

Temperature Programmed Reduction

The reduction process of Mo/NiO, Zr/NiO, W/NiO, Ce/NiO, Co/NiO and NiO catalysts in the CO atmosphere was studied by using CO-TPR (Figure 1) under a flow of 40% CO in N_2 (20 mL·min^{-1}) in a non-isotherm (40-700°C, 10°C·min^{-1}). TPR analysis profile was obtained from the reduction process of NiO catalysts added with various transition metals compared with undoped NiO catalysts. The reduction reaction for undoped NiO occurred at the temperature of 384°C. Referring to the study by Sharma et al. (1997), Alizadeh et al. (2007) and Krasuk & Smith (1972), responses to NiO catalyst reduction using C, H_2 and CO as reducing agents occurred through only one step of the reduction reaction, i.e., $NiO \rightarrow Ni^0$.

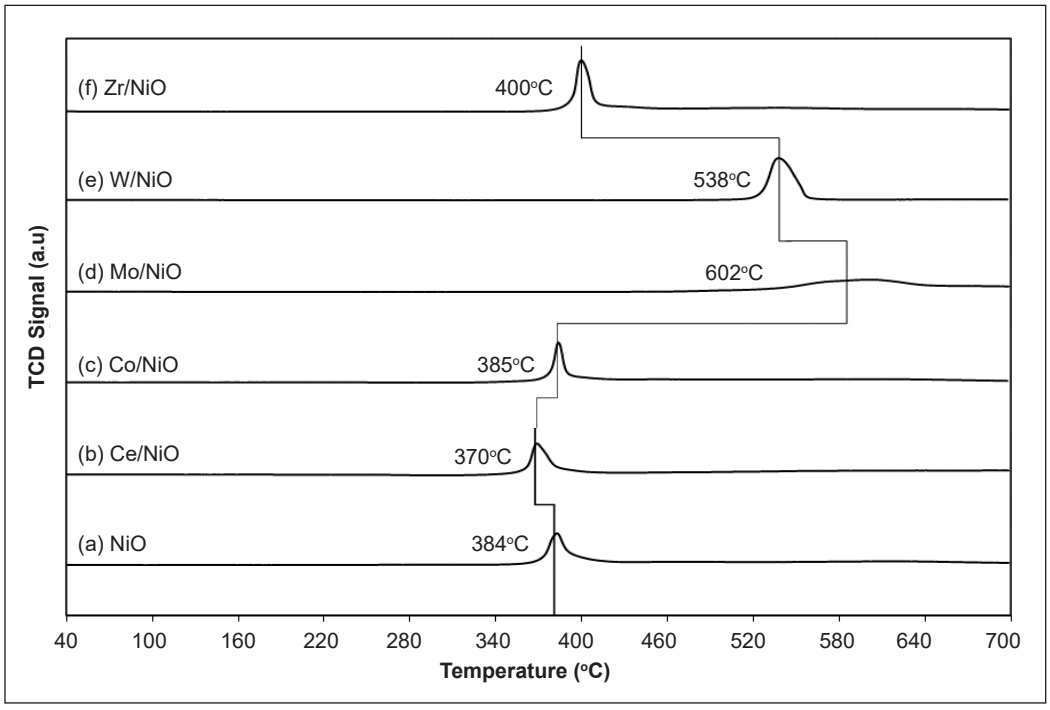

Figure 1. The TPR profile for 3% bt. various other metals upward of NiO is modified under a flow of 40% CO in N_2 (20 mL·min^{-1}) in a non-isotherm (40-700°C, 10°C·min^{-1})

The results of the TPR analysis shown in Figure 1 describe a change in the position of the decreased peak for all 3% of the metal loads to NiO. The 3% wt./wt. metal loading is chosen to screen the effectiveness of transition metal doped NiO and observe whether this percentage is sufficient to reduce temperature/behaviour. Although the 3% metal loads of the transition metal doped NiO was small, it gave a very significant reduction effect. It was found that only Ce/NiO gave the lowest reduction temperature of 370°C compared

to the NiO catalyst of 384°C. It is most likely due to the metal-metal interaction between Ce and NiO because Ce particles are more likely to disperse evenly on the NiO surfaces (Dzakaria et al., 2021), and the increase in surface area on a Ce/NiO catalyst facilitates the reduction reaction to occur quickly. At the same time, other metal loads such as W/NiO, Mo/NiO, Co/NiO and Zr/NiO showed a higher reduction temperature than NiO catalysts. It is due to the formation of new compounds or more stable nickel alloys and, in turn, can further slow down the action counter-decline.

Crystallinity Analysis Using XRD

XRD analysis was performed in the 2θ range between 10° - 80° for NiO and modified catalysts consisting of Mo/NiO, Zr/NiO, W/NiO, Ce/NiO and Co/NiO at 3% loads, respectively (Figures 2). The XRD pattern for NiO indicates a stoichiometric cubic-shaped phase (JCPDS 00-047-1049). The addition of Ce, Co and W at 3% (wt./wt.) showed no significant changes in crystal structure due to the addition of a small amount of Ce, Co and W metals or the Ce, Co and W compounds existed in amorphous form so that they could not be detected using XRD techniques. Moreover, the addition of Ce, Co and W may make these metals completely dispersed on the surface of NiO. Subsequently, adding Mo to NiO indicates a new diffraction pattern of MoO_3 as the orthorhombic phase (JCPDS 01-878-4613). At the same time, the addition of W showed a slight presence of WO_3 as the triclinic phase (JCPDS 00-020-1323) in addition to the major peak of NiO.

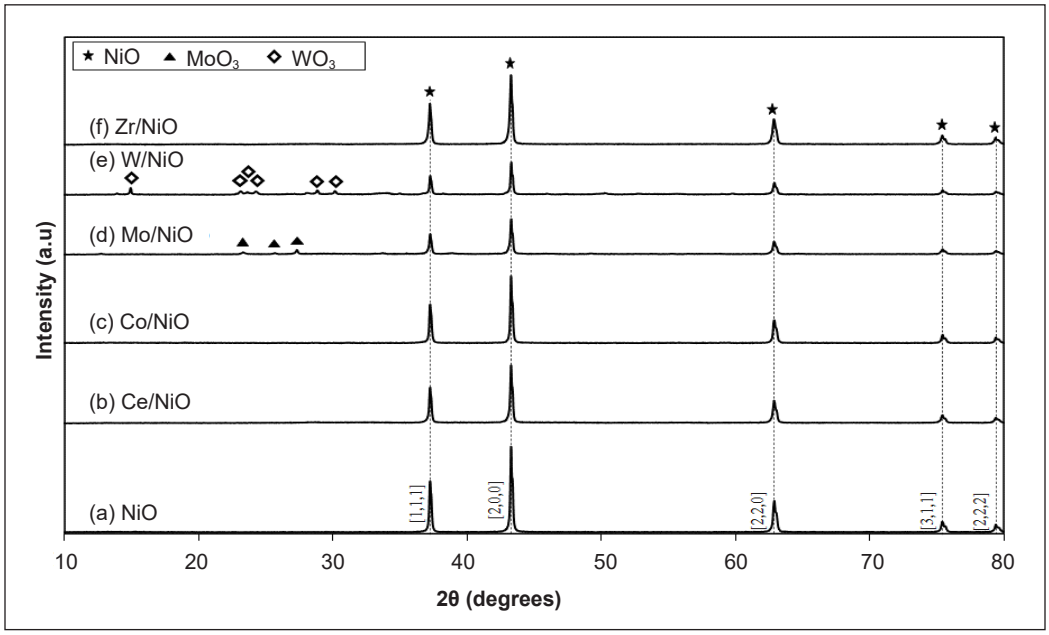

Figure 2. XRD diffractogram of (a) NiO; (b) Ce/NiO; (c) Co/NiO; (d) Mo/NiO; (e) W/NiO/SiO2 and (f) Zr/NiO after calcined at 400ºC for 4 hours

After the reduction reaction, the samples were collected for analysis using the XRD technique to understand the crystallinity properties of the modified NiO catalyst. This XRD analysis was performed on a modified NiO catalyst that underwent a reduction reaction using CO gas as the reduction agent under non-isothermal reduction conditions (40–700°C, 10°C·min^{-1}) under a flow of 40% CO in N_2 (20 mL·min^{-1}). XRD diffractograms were performed in the 2θ range between 10°–80° for NiO catalysts and modified NiO catalysts at 3% wt. The various metals doped NiO after the reduction reaction are shown in Figure 3. The XRD diffraction pattern of the NiO catalyst after the reduction reaction shows a change in which the cubic-shaped NiO (JCPDS 00-047-1049) is completely reduced to cubic-shaped NiO (JCPDS 01-087-9414) with a 2θ value of 44.5°, 51.9°, 76.4° representing the lattice plane (1,1,0), (2,0,0), (2,2,0) and no other compound. When the addition of 3% bt. multi-metal loading was performed on the NiO catalyst, and the XRD diffraction pattern showed only Mo/NiO and W/NiO small peak formation for MoO_2 (JCPDS 01076-1807) and $WO_{2.72}$ (JCPDS 01-084-1516). At the same time, other modified NiO catalysts did not show any formation of new phase peaks other than Ni phase peaks of different intensities. Due to the low content of the metals, peaks from other metals are expected to be scattered on the surface of the NiO catalyst in the form of an amorphous or nano-shaped structure.

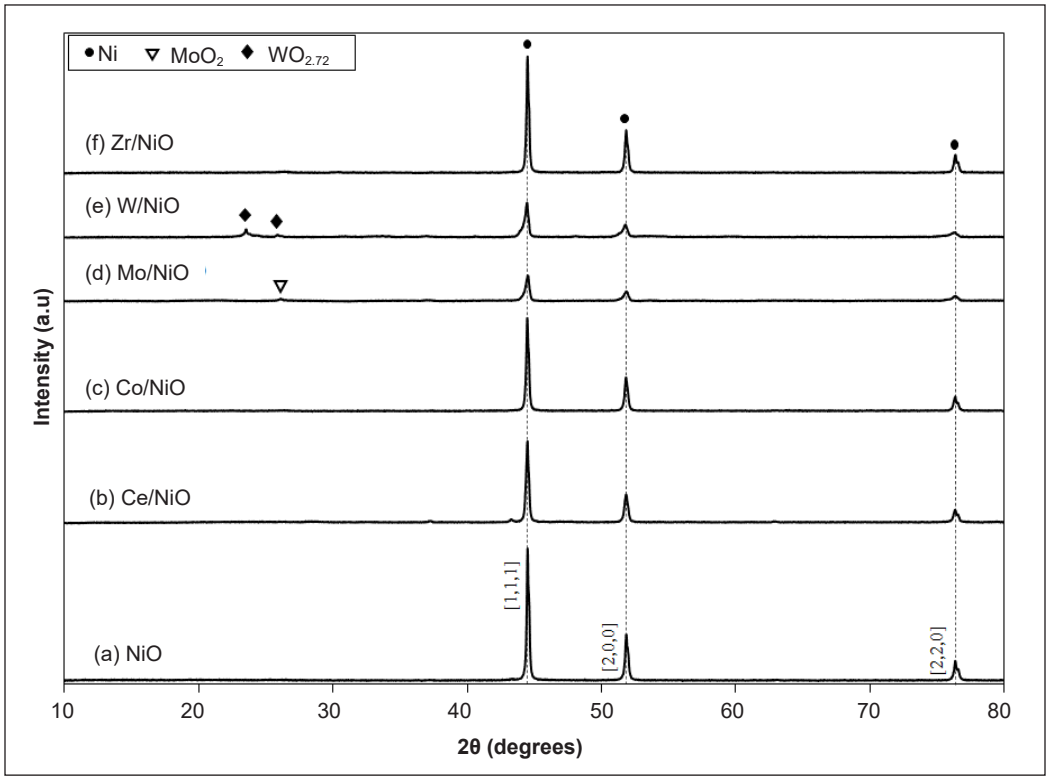

Figure 3. XRD diffractograms (a) NiO; (b) Ce/NiO; (c) Co/NiO; (d) Mo/NiO; (e) W/NiO and (f) Zr/NiO after reduction at 40-700ºC, 10°C·min^{-1}

Physical Surface Analysis

The textural properties of the catalysts were studied through N_2 adsorption-desorption isotherms (Figure 4) and its parameters, such as BET surface area, pore volume and average pore diameter (Table 1). The adsorption isotherms are associated with type III according to IUPAC adsorption isotherms of classification, whereas hysteresis H4 type is characteristic of macroporous materials. The hysteresis, proven based on the isotherms associated with narrow slit pores, is observed (Sing et al., 1985; Othman, 2012).

The parameters of BET surface area, pore volume and average pore diameter for the catalysts are shown in Table 1. The plot of the isotherm of N_2 adsorption for 3% wt. transition metals doped NiO are shown in Figure 4. Based on the IUPAC classification, the shape of the NiO catalyst isothermal curve is a type III mesoporous isotherm with H4 hysteresis. This type III isotherm shows that NiO catalysts have multilayer adsorption properties on non-porous or macroporous materials. Catalysts having this type of isotherm are characterised as adsorption occurs when the interaction between the adsorbed material and the first adsorbent layer is stronger than the interaction of the adsorbed material with the surface of the adsorbent material. Meanwhile, the hysteresis property of H4 has the characteristic of a wide slope between the adsorption and desorption plots that is wide

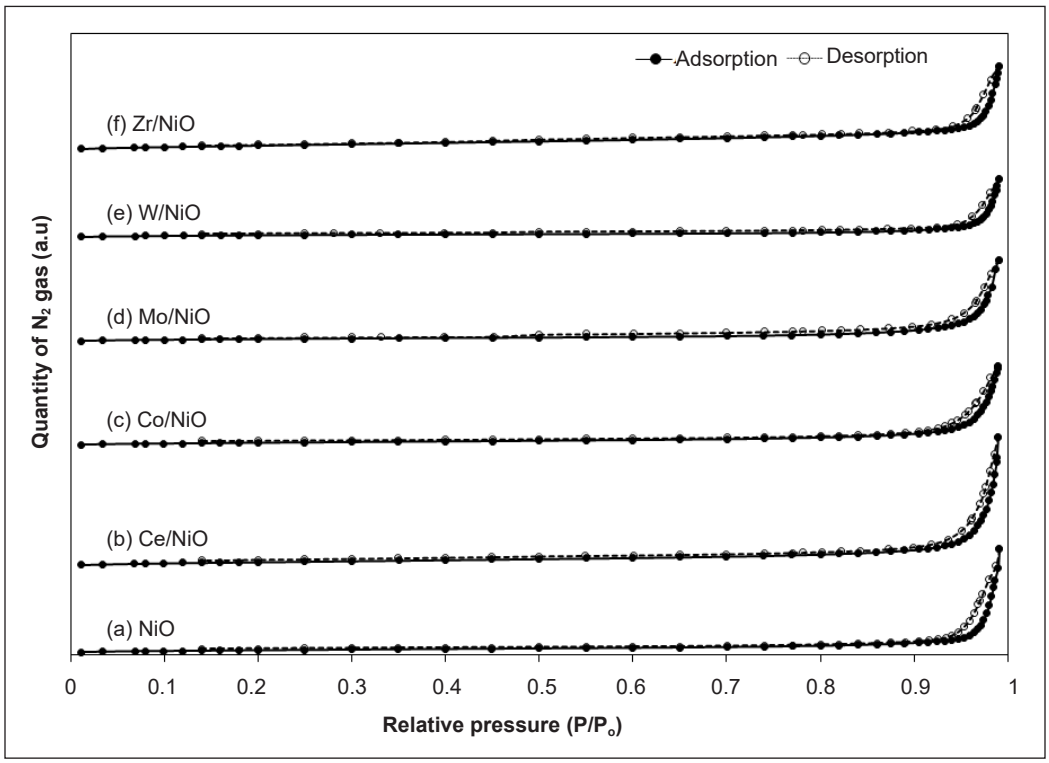

Figure 4. N_2 adsorption-desorption isotherms for (a) NiO, (b) Ce/NiO, (c) Co/NiO, (d) Mo/NiO, (e) W/NiO and (f) Zr/NiO

and covers a large part of the relative pressure area range (P/P_0). The 3% metal loading of various metals shows the same type of isotherm and hysteresis. Apart from this isothermal plot, it was found that all the modified NiO catalyst materials were mesoporous with the addition of 3% metal loading.

Table 1 shows the values of surface area (S_{BET}), pore diameter (D_{pore}) and modified volume (V_{pore}) and NiO catalysts. The results showed significant changes in the surface area, volume and diameter of the pores from the samples studied. It was because each addition of a different metal to the NiO catalyst surfaces had a different particle size, resulting in different textural properties. The surface area of the NiO catalyst was 4.5 m^2/g with pore diameter and volume of 40.6 nm and 0.030 cm^3/g, respectively. The NiO catalysts with such surface area value are considered a material with a very low surface area. NiO samples are highly crystalline due to having a low surface area. In Table 1, Zr/NiO has a higher surface area than other metals doped NiO but a slightly higher reduction temperature than Ce/NiO. Salleh et al. (2015) and Vazinishayan et al. (2018) stated that ZrO_2 has higher BET surface areas than NiO. It suggests that more active sites may be attributed to the higher temperature reduction of NiO after doping.

Overall, the addition of different metals, namely Ce, Co, Mo, W and Zr, showed a slight increase in the surface area compared to undoped NiO. The increase in surface area is likely due to the increase in the surface area contributed by the effect of metal oxides added via impregnation. Some additional metal oxides were expected to have partially filled the NiO mesopores and partially formed a new surface outside the NiO pores. This phenomenon is due to the larger additional cluster metal size and the higher quantity of metal than the pore volume. Metallic materials outside the pores can usually add to the surface area of the catalyst material (Zurina, 2015). Nevertheless, the volume and diameter of the pores showed less significant changes after adding other metals.

Table 1
Surface area, pore size and pore volume of NiO catalyst and various transition metal doped NiO

Catalyst	S_{BET} (m^2/g)	D_{pore} (nm)	V_{pore} (cm^3/g)
NiO	4.5	40.6	0.030
Ce/NiO	6.8	32.1	0.038
Co/NiO	4.8	29.0	0.027
Mo/NiO	4.8	33.1	0.033
W/NiO	5.2	29.2	0.017
Zr/NiO	8.9	16.1	0.027

The pore size distribution was computed using N_2 adsorption-desorption isotherm data to apply with the Barrett-Joyner-Halenda (BJH) model. Figure 5 shows the pore size distribution of the various metals doped NiO catalysts, with the inset picture showing

the enlarged scale at 20 to 60 Å (2-6 nm). The catalysts showed a significant change in pore size distribution after being doped with various metals. The inset figure in Figure 5 indicates that Mo/NiO has the highest pore size distribution in the 30 to 42 Å (3-4.2 nm) compared to the rest of the NiO-doped catalysts. Undoped NiO was not observed in the pore size distribution of the 20-60 Å (2-6 nm) region. Thus, the additive metals contribute to the changes in pore size distribution at the mesopore region. In general, the presence of additive metals contributes to a higher surface area than NiO (Table 1). It is due to each metal particle having its pores as well.

Various pore size distribution patterns were observed at the 300 to 1800 Å (30-180 nm) region. The undoped NiO only exhibited pore size distribution at mesopore to macropore region around 300 to 1800 Å (30-180 nm). A mesopore region is found in the range of 20 to 500 Å (2-50 nm), whereas a macropore region is located in the range larger than 500 Å (50 nm) (Hakim, Tahari et al., 2015; Hakim et al., 2016). The undoped NiO has a larger pore size distribution at 300 to 1100 Å (30-110 nm) compared to Co/NiO, W/NiO, Mo/NiO and Zr/NiO. It could be attributed to additive metals in smaller sizes that are partially embedded into NiO pores of this region. Meanwhile, the Ce/NiO possesses Ce particles of larger sizes, which possibly makes Ce particles the only particles deposited on NiO surfaces. Furthermore, at 600 to 1500 Å (60-150 nm), the Ce/NiO showed the highest and broadest distribution. Therefore, the high surface area of the Ce/NiO catalyst is attributed to the mesopore and macropore regions.

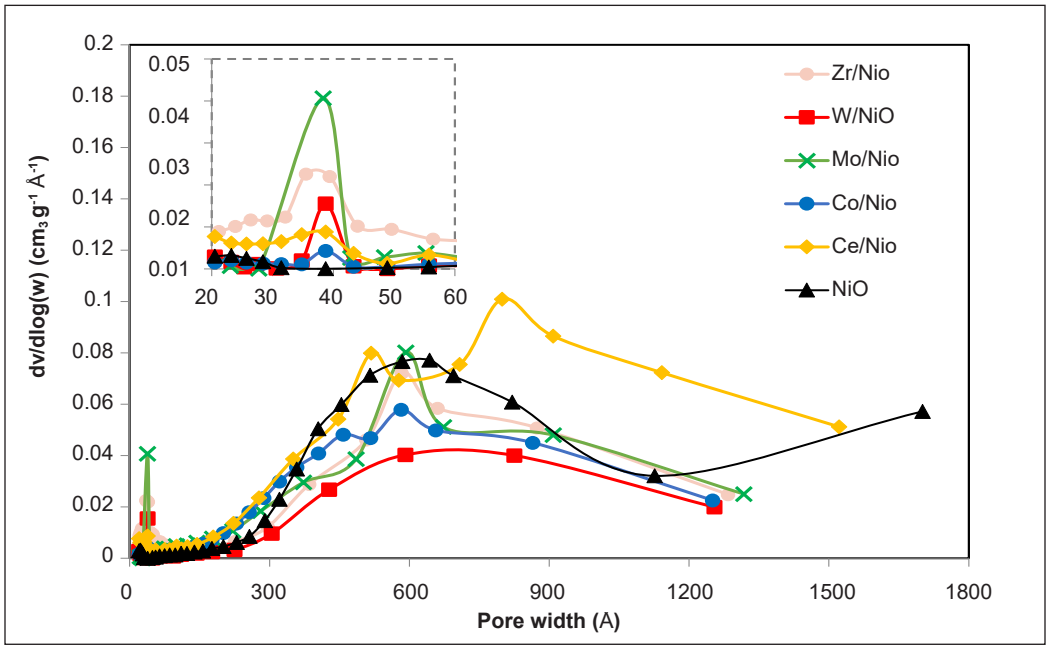

Figure 5. Pore size distribution of the various metals doped NiO catalysts with the inset picture showing the enlarged scale at 20 to 60 Å (2-6 nm)

CONCLUSION

The reduction behaviour of Mo/NiO, Zr/NiO, W/NiO, Ce/NiO, Co/NiO and undoped NiO catalysts in the CO atmosphere was investigated and compared using the TPR technique and characterised by XRD and N_2 gas adsorption-desorption analysis (BET). This research revealed that the reduction reaction obeyed the consecutive mechanism, and NiO was reduced to Ni completely. The 3% Ce/NiO possessed a higher surface. Furthermore, adding Ce to NiO enhanced a lower reduction temperature compared to adding Co, Mo, W and Zr. Adding Ce to the NiO shifted the TPR peaks to the lower temperature. It can be concluded that the reduction temperature of NiO decreases by the Ce with 3% Ce loading, which is sufficient to reduce NiO to Ni at 370°C. It is mainly ascribed to ceria's intricate redox and O^{2-} -defect chemistry capable of transporting oxygen species and exhibiting a strong metal-support interaction favouring a higher Ni dispersion. The Ce changes the coordination environment of nickel and the strength of Ni-O bonds, leading to a decrease in the reduction temperature of doped NiO.

ACKNOWLEDGEMENT

The publication fee is supported by UPM-Kyutech International Symposium on Applied Engineering and Sciences 2022 (SAES2022) and Universiti Putra Malaysia.

REFERENCES

Ahmad T., Pandey V., Saddam Husain M., Adiba, & Munjal S. (2022). Structural and spectroscopic analysis of pure phase hexagonal wurtzite ZnO nanoparticles synthesized by sol-gel. *Materials Today Proceeding. 49,* 1694-1697. https://doi.org/10.1016/j.matpr.2021.07.456

Alizadeh, R., Jamshidi, E., & Ale-Ebrahim, H. (2007). Kinetic study of nickel oxide reduction by methane. *Chemical Engineering and Technology 30*(8), 1123-1128. https://doi.org/10.1002/ceat.200700067

Anastasios I. T., Nikolas D. C., Ioannis V. Y., & Maria A. G. (2021). Bimetallic Ni-Based Catalysts for CO_2 Methanation: A Review. *Nanomaterials*, *11*(28), 1-34.

Charisiou, N. D., Papageridis, K. N., Tzounis, L., Sebastian, V., Hinder, S. J., Baker, M. A., AlKetbi, M., Polychronopoulou, K., & Goula, M. A. (2019). Ni supported on CaO-MgO-Al_2O_3 as a highly selective and stable catalyst for H_2 production via the glycerol steam reforming reaction. *International Journal of Hydrogen Energy*, *44*(1), 256-273. https://doi.org/10.1016/j.ijhydene.2018.02.165

Charisiou, N. D., Tzounis, L., Sebastian, V., Hinder, S. J., Baker, M. A., Polychronopoulou, K., & Goula, M. A. (2019). Investigating the correlation between deactivation and the carbon deposited on the surface of Ni/Al_2O_3 and Ni/La_2O_3 -Al_2O_3 catalysts during the biogas reforming reaction. *Applied Surface Science*, *474*, 42–56. https://doi.org/10.1016/j.apsusc.2018.05.177

Cho D. Y., Luebben M., Wiefels S., Lee K. S., & Valov. I. (2017). Interfacial metal-oxide interactions in resistive switching memories. *ACS Applied Materials & Interfaces*, *9*(22), 19287-19295. https://doi.org/10.1021/acsami.7b02921

Dzakaria, N., Lahuri, A. H., Tengku Saharuddin, T. S., Samsuri, A, Salleh, F., Wan Isahak, W. N. R., Yusop, M. R., & Yarmo, M. A. (2021). Preparation of cerium doped nickel oxide for lower reduction temperature in carbon monoxide atmosphere. *Malaysian Journal of Analytical Sciences, 25*(3), 521-531.

Dzakaria, N., Tahari, M. N. A., Samidin, S., Tengku Saharuddin, T. S., Salleh, F., Lahuri, A. H., & Yarmo, M. A. (2020). Effect of cobalt on nickel oxide toward reduction behaviour in hydrogen and carbon monoxide atmosphere. *Material Science Forum*, *1010*, 373-378. https://doi.org/10.4028/www.scientific.net/MSF.1010.373

Dzakaria, N., Samsuri, A., Halim, A., M. A., Saharuddin, T. S. T., Tahari, M. N. A., Salleh, F., Yusop, M. R., Isahak, W. N. R. W., Hisham, M. W. M., & Yarmo, M. A. (2020). Chemical reduction behavior of zirconia doped to nickel at different temperature in carbon monoxide atmosphere. *Indonesian Journal of Chemistry*, *20*(1), 105-112. https://doi.org/10.22146/ijc.40891

Fakeeha A., Ibrahim A. A., Aljuraywi H., Alqahtani Y., Alkhodair A., Alswaidan S., Abasaeed A. E, Kasim S. O., Mahmud S., & Al-Fatesh A. S. (2020). Hydrogen production by partial oxidation reforming of methane over Ni catalysts supported on high and low surface area alumina and zirconia. *Processes*, *8*(5), Article 499. https://doi.org/10.3390/pr8050499

Farber S., Ickowicz D. E., Melnik K., Yudovin-Farber I., Recko D., Rampersaud A., & Domb A. J. (2014). Surface functionalization of magnetic nanoparticles formed by self-associating hydrophobized oxidized dextrans. *Journal of Nanoparticle Research*, *16*, Article 2425. https://doi.org/10.1007/s11051-014-2425-z

Hasannejad, H., Shahrab, T., & Jafarian, M. (2012). Synthesis and properties of high corrosion resistant Ni-cerium oxide nano-composite coating. *Material Corrosion*, *64*(12), 1104-1113. https://doi.org/10.1002/maco.201106484

Hakim. A., Tahari, M. N. A., Marliza, T. S., Wan Isahak, W. N. R., Yusop, M. R., Hisham, W. W. M., & Yarmo, M. A. (2015). Study of CO_2 adsorption and desorption on activated carbon supported iron oxide by Temperature Programmed Desorption. *Jurnal Teknologi (Sciences & Engineering)*, *77*(33), 75-84. https://doi.org/10.11113/jt.v77.7010

Hakim, A., Isahak, W. N. R. W., Yusop, M. R., Tahari, M. N. A., Hisham, M. W. M., & Yarmo, M. A. (2015). Temperature programmed desorption of carbon dioxide for activated carbon supported nickel oxide: The adsorption and desorption studies. *Advanced Materials Research*. *1087*, 45-49. https://doi.org/10.4028/www.scientific.net/AMR.1087.45

Hakim, A., Yarmo, M. A., Marliza, T. S., Tahari, M. N. A., Samad, W. Z., Yusop, M. R., Hisham, W. W. M., & Dzakaria, N. (2016). The influence of calcination temperature on iron oxide (α-Fe_2O_3) towards CO_2 adsorption prepared by simple mixing method. *Malaysian Journal of Analytical Sciences*, *20*(6), 1286-1298. http://dx.doi.org/10.17576/mjas-2016-2006-07

Kaiser M. (2004). Semiconductor-to-metallic transition in Cu-substituted Ni - Mn ferrite. *Physica Status Solidi*, *201*(14), 3157-3165. https://doi.org/10.1002/pssa.200406861

Khan, I., Saeed, K., & Khan I. (2019), Nanoparticles: Properties, applications and toxicities. *Arabian Journal of Chemistry, 12*(7)*,* 908-931. https://doi.org/10.1016/j.arabjc.2017.05.011

Krasuk, J. H., & Smith, J. M. (1972). Kinetics of reduction of nickel oxide with carbon monoxide. *AIChE Journal 18*(3), 506-512. https://doi.org/10.1002/aic.690180308

Lahuri, A. H., Ling, N. K. M., Rahim, A. A., & Nordin, N. (2020). Adsorption kinetics for CO_2 capture using cerium oxide impregnated on activated carbon. *Acta Chimica Slovenica*, *67*(2), 570-580. http://dx.doi.org/10.17344/acsi.2019.5572

Lahuri, A. H., Yusuf, A. M., Adnan, R., Rahim, A. A., Tajudee, N. F. W., & Nordin, N. (2022). Kinetics and thermodynamic modeling for CO_2 capture using NiO supported activated carbon by temperature swing adsorption. *Biointerface Research in Applied Chemistry*, *12*(3), 4200-4219. https://doi.org/10.33263/BRIAC123.42004219

Lv, C., Xu, L., Chen, M., Cui, Y., Wen, X., Li, Y., Wu, C.E., Yang, B., Miao, Z., & Hu, X. (2020). Recent progresses in constructing the highly efficient Ni based catalysts with advanced low-temperature activity toward CO_2 methanation. *Frontiers in Chemistry*, *8*, Article 269. https://doi.org/10.3389/fchem.2020.00269

Othman, Z. A. (2012). A review: Fundamental aspects of silicate mesoporous materials. *Materials, 5*(12), 2874-2902. https://doi.org/10.3390/ma5122874

Oudejans D., Offidani M., Constantinou A., Albonetti S., Dimitratos N., & Bansode A. (2022). A comprehensive review on two-step thermochemical water splitting for hydrogen production in a redox cycle. *Energies*, *15*(9), Article 3044. https://doi.org/10.3390/en15093044

Pandey V., Adiba, Munjal S., & Ahmad T. (2020). Optical properties and spectroscopic investigation of single phase tetragonal Mn_3O_4 nanoparticles. *Material Today Proceeding*, *26*, 1181-1183. https://doi.org/10.1016/j.matpr.2020.02.238

Papageridis, K. N., Charisiou, N. D., Douvartzides, S., Sebastian, V., Hinder, S. J., Baker, M. A., AlKhoori, S., Polychronopoulou, K., & Goula, M. A. (2020). Promoting effect of CaO-MgO mixed oxide on Ni/γ-Al_2O_3 catalyst for selective catalytic deoxygenation of palm oil. *Renewable Energy*, *162*, 1793-1810. https://doi.org/10.1016/j.renene.2020.09.133

Parkinson, G. S., Mulakaluri, N., Losovyj, Y., Jacobson, P., Pentcheva, R., & Diebold, U. (2010). Semiconductor-half metal transition at the Fe_3O_4 (001) surface upon hydrogen adsorption. *Physical Review B*, *82*, Article 125413. https://doi.org/10.1103/PhysRevB.82.125413

Rebello, A., & Adeyeye, A. O. (2016). Robust electric-field tunable opto-electrical behavior in Pt-NiO-Pt planar structures. *Scientific Reports*, *6*, Article 28007. https://doi.org/10.1038/srep28007

Salleh, F., Saharuddin, T. S. T., Samsuri, A., Othaman, R., & Yarmo, M. A. (2015). Effect of zirconia and nickel doping on the reduction behavior of tungsten oxide in carbon monoxide atmosphere. *International Journal of Chemical Engineering Application*, 6(*6*), 389-394. https://doi.org/10.7763/ijcea.2015.v6.516

Sharma, K., Vastola, F. J., & Walker, P. L. 1997. Reduction of nickel oxide by carbon: III. Kinetic studies of the interaction between nickel oxide and natural graphite. *Carbon, 35*(4), 535-541. https://doi.org/10.1016/S0008-6223(97)83728-1

Siakavelas, G. I., Charisiou, N. D., AlKhoori, S., AlKhoori, A. A., Sebastian, V., Hinder, S. J., Baker, M. A., Yentekakis, I. V., Polychronopoulou, K., & Goula, M. A. (2021). Highly selective and stable nickel catalysts supported on ceria promoted with Sm_2O_3, Pr_2O_3 and MgO for the CO_2 methanation reaction. *Applied Catalysis B: Environmental*, *282*, Article 119562. https://doi.org/10.1016/j.apcatb.2020.119562

Sing, K. S. W., Everett, D. H., Haul, R. A. W., Moscou, L., Pierotti, R. A., & Rouquerol, J. (1985). Reporting physisorption data for gas/solid systems with special reference to the determination of surface area and porosity. *Pure and Applied Chemistry, 57*(4), 603-619. https://doi.org/10.1351/pac198557040603

Sun, J., Zhang, X., Jin, M., Xiong, Q., Wang, G., Zhang, H., & Zhao, H. (2020). Robust enhanced hydrogen production at acidic conditions over molybdenum oxides-stabilized ultrafine palladium electrocatalysts. *Nano Research*, *14*, 268-274. https://doi.org/10.1007/s12274-020-3083-3

Tsiotsias, A. I., Charisiou, N. D., Yentekakis, I. V., & Goula, M. A. (2020). The role of alkali and alkaline earth metals in the CO_2 methanation reaction and the combined capture and methanation of CO_2. *Catalysts*, *10*(7), Article 812. https://doi.org/10.3390/catal10070812

Vazinishayan, A., Lambada, D. R., Yang, S., Zhang, G., Cheng, B., Woldu, Y. T., Shafique, S., Wang, Y., & Anastase, N. (2018). Effects of mechanical strain on optical properties of ZnO nanowire. *AIP Advances*, *8*(2), Article 025306. https://doi.org/10.1063/1.5016995

Wondimu, T. H., Bayeh, A. W., Kabtamu, D. M., Xu, Q., Leung, P., & Shah, A. A. (2022). Recent progress on tungsten oxide-based materials for the hydrogen and oxygen evolution reactions. *International Journal of Hydrogen Energy*, *47*(47), 20378-20397. https://doi.org/10.1016/j.ijhydene.2022.04.226

Zheng, J., Dong, Y., Wang, W., Ma, Y., Hu, J., Chen, X., & Chen, X. (2013). In situ loading of gold nanoparticles on Fe_3O_4@SiO_2 magnetic nanocomposites and their high catalytic activity. *Nanoscale*, *5*(11), 4894-4901. https://doi.org/10.1039/C3NR01075A

Zurina, S. W. (2015). Conversion of glycerol to 1,2-propanadiol and methanol by hydrogenolysis and sub-critical fluid techniques using fluorine-doped tin oxide (FTO) catalyst. Universiti Kebangsaan Malaysia.